Aeroacoustic Optimization of a Low Speed Fan

João Miguel Rebelo Branco
joao.r.branco@ist.utl.pt

Instituto Superior Técnico, Lisboa, Portugal

June 2015

Abstract

As the use of air conditioning systems has increased in the recent decades due to the growth of the purchasing power in the developed world and the confort they provide, so has the awareness regarding the negative health impacts of these systems also increased. Many studies were conducted to predict and minimize the noise of the fans present in most of these systems. In this work, a noise prediction framework based on the Blade Element Momentum method for aerodynamic prediction was coupled to the empirical aeroacoustic models based on the works of Carolus et al (2007) and Brooks et al (1989) and to XFOIL for boundary layer parameter calculations. This framework was validated against experimental data of a known axial impeller and an existing air conditioning fan model was analyzed and its baseline noise characteristics were evaluated. A blade parameterization method was developed where the chord and twist distributions and airfoil sections were described by Bézier curves. A parametric study to determine the impact of fan diameter and blade number on the produced noise was conducted. The aeroacoustic code was coupled to the optimization framework pyOpt, and by using the NSGA-II genetic algorithm, a set of single and multi-objective optimizations, with chord, twist and curvature as design variables were performed on the baseline fan and on the minimum noise fan resultant from the parametric study. The optimal solutions indicated a maximum reduction of 4.1% in noise and a maximum increase of 5.3% in efficiency. Introducing diameter and blade number changes, a significant noise reduction is possible but with a moderate aerodynamic penalty.
Keywords: Aeroacoustic Design, Noise Reduction, Air Conditioning, Multi-objective Optimization, Genetic Algorithms

1. Introduction

In the modern age, air conditioning systems have become so common, that they are already a part of the urban landscape. Due to their widespread use, several studies regarding the negative environmental and public health impact of the air conditioning systems were conducted, including the impact of the noise [1]. These hazardous effects motivated, in some metropolitan areas, the creation of noise legislation to impose limits on the noise produced by air conditioning systems. The fan located in the outdoor units of these systems is responsible for the greater portion of the produced noise, which is mostly aerodynamic noise.

The main objective of this work was to optimize the geometry of an already existing air conditioning fan in order to minimize the produced noise, while maximizing the fan aerodynamic efficiency, by adapting an already tested custom wind turbine aeroacoustic tool to an axial fan case.

A bibliographical review of the most used and reliable aeroacoustic models was performed and some of them were implemented in the code and validated using experimental results from known fan data. A parametrization model to describe the blade geometry using Bézier curves was also developed. The aeroacoustic code was coupled to an optimization framework in order to proceed to the single and multi-objective optimization of the fan geometry.

2. Theoretical Models

In this section, an overview of the aerodynamic and aeroacoustic models used in this work is presented and briefly discussed.

2.1. Aerodynamic Model

The aerodynamic model predicts the fan aerodynamic performance besides providing the necessary data for the aeroacoustic model, such as the radial distribution of velocity, effective angle of attack, Reynolds number, among others. This model relies upon the implementation of a Blade Element Momentum method [6], with correction for hub and tip losses.

The aerodynamic data required by the BEM method is supplied in form of aerodynamic polars, which can be user-supplied or it can be automati-

cally calculated by XFOIL. This data is subjected to corrections for 3D effects based on the stall delay model by Du and Selig [5]. The data is extrapolated for angles outside of the calculated range using a method developed by Viterna and Janetzke [11].

The fan efficiency will be considered as an indicator of the aerodynamic performance and it will be computed through the ratio between the power transfered to the flow and the power consumed by the fan and it is expressed by

$$\eta = \frac{TV}{Q\omega} \quad , \tag{1}$$

where T is the total thrust to which the fan is subjected, V is the flow axial velocity, Q is the total fan torque and ω is the rotational speed.

2.2. Aeroacoustic Model

The used aeroacoustic model takes into account the turbulent inflow noise and the five mechanisms of the airfoil self-noise.

Turbulent Inflow Noise The turbulent inflow noise is produced by the turbulence of the flow passing through the fan, which creates zones of recirculating flow and eddies of different sizes and intensities. When these turbulent eddies make contact with the fan blades, a broadband noise is produced.

A semi-empiric method developed specifically for axial flow fans by Carolus and Schneider [4] was used to predict the turbulent inflow noise. The spectral density of the acoustic power of Z uncorrelated broadband sources is given by

$$PSD_W(f) = \frac{\pi}{4}\frac{Z}{\rho c_0^2}\frac{f}{r_a(1-({}^{r_i}/_{r_a})^2)^2}PSD_F(f) \tag{2}$$

where r_i is the hub radius, $r_a = \dfrac{D}{2}$, D is the fan diameter, ρ is the air density, c_0 is the speed of sound and f is the frequency of the noise to be predicted. The force fluctuation on a blade, $PSD_F(f)$ is expressed in terms of the fluctuating pressure surface distribution PSD_{sp} and the correlation area A_c,

$$PSD_F(f) = \iint_A PSD_{sp}(f,\xi_1,\xi_3)A_c(f,\xi_1,\xi_3)\mathrm{d}\xi_1\mathrm{d}\xi_3 \ , \tag{3}$$

where ξ_1 and ξ_3 are coordinates of the rotating frame of reference defined in the model.

In this work, the integral in equation (3) is evaluated numerically in each blade element by multiplying the integrand with the element projected area, being the area computed by the Simpson's rule numerical integration scheme. The fluctuating pressure surface distribution PSD_{sp} is given by

$$PSD_{sp} = \frac{1}{4}(0.9\pi)^2\rho^2 w_1^2 PSD_{w2} \quad , \tag{4}$$

with w_1 being the effective velocity of the flow approaching the blade element. PSD_{w2} is the spectral density of the speed fluctuations of the flow perpendicular to the blade surface and it can be approximated by the spectral density of the axial flow velocity PSD_{cx}, which is expressed by the non-dimensional spectrum $PSDL^*_{cx}$

$$PSDL^*_{cx} = 10\log\left(\frac{PSD_{cx}}{c_x Tu^2 \Lambda_x}\right) dB \quad , \tag{5}$$

where Tu and Λ_x are the turbulence intensity and length scale, respectively and c_x is the axial flow velocity.

There are several published empirical correlations which give this spectrum, being chosen a polynomial curve fit to an extensive series of measurements by Költzsch in [2]

$$PSDL^*_{cx}(Sr_{\Lambda x}) = \sum_{k=1}^{4} a_k(\log(Sr_{\Lambda x}))^{k-1} dB \quad , \tag{6}$$

with $a_1 = -9.784$, $a_2 = -19.001$, $a_3 = -5.548$ and $a_4 = -0.06$. The Strouhal number $Sr_{\Lambda x}$ is defined as $Sr_{\Lambda x} = \frac{f\Lambda_x}{c_x}$.

The authors of this model performed a statistical study of the turbulence parameters Tu and Λ_x and obtained different ranges of values for various intake conditions, ranging from Natural Inflow (NI), where there is no type of inlet grid in the system, to a Turbulence Control Screen (TCS), which is a device used to generate a low turbulence flow in the intake nozzle. The values for these parameters for different inlet conditions is presented in table 1.

Configuration type	Λ_x (mm)	Tu (%)
RPG1	9-16	12.5-20.9
Natural Inflow (NI)	12-35	0.6-14.2
Honeycomb (HC)	3-15	1.4-13.5
RPG2	10-18	16.7-21.3
TCS	7-28	0.4-8
TCS + BLR	1-8	0.5-5

Table 1: Turbulence parameters for multiple inflow configurations [4].

The correlation area A_c is given by [10]

$$A_c = \frac{w_1}{2\pi f} \quad . \tag{7}$$

Airfoil Self-Noise Airfoil self noise is a consequence of the interaction between the self-produced boundary layer and wake and the airfoil itself. Brooks, Pope and Marcolini [3] performed an extensive study on the airfoil self-noise and found that it can be divided in five separate mechanisms:

1. Turbulent boundary layer trailing edge noise,
2. Separation-stall noise,
3. Laminar boundary layer vortex shedding noise,
4. Trailing edge bluntness vortex shedding noise,
5. Tip vortex formation noise.

The 1/3 octave noise spectrum produced by the first three mechanisms can be predicted by semi empirical scaling laws given by BP&M, in the form

$$L_{p,i} = 10\log\left(\frac{\delta_i M^{f(i)} L\bar{D}}{r_e^2}\right) + F_i(St) + G_i(Re), \quad (8)$$

where δ_i can be either the boundary layer thickness or displacement thickness, and $f(i)$ a value which depends on the noise mechanism. The terms $F_i(St)$ and $G_i(Re)$ are spectral shape functions based on the Strouhal number St and Reynolds number Re, respectively, which are different for each mechanism. Trailing edge bluntness vortex shedding and tip vortex formations noises are also predicted in a similiar way, with the first using spectral shape functions based on the trailing edge solid angle Ψ_{TE} and trailing edge thickness h.

Total Fan Noise Prediction The total fan noise is computed by dividing the blade in n noise elements. In each of these elements, the two-dimensional noise and turbulent inflow noise prediction is performed and the total sound pressure level generated by the fan is the summation of the noise from each blade element $L_{p,i}$,

$$L_{p,total} = 10\log\left(\frac{N_B}{N_{az}}\sum_i 10^{\frac{L_{p,i}}{10}}\right), \quad (9)$$

where N_{az} is the number of azimuthal positions at which the blade is computed and N_B is the number of blades. The Overall Sound Pressure Level (OASPL) can be obtained by summing the noise levels at every frequency,

$$OASPL = 10\log\left(\sum_i 10^{\frac{L_{p,j}}{10}}\right), \quad (10)$$

where $L_{p,j}$ is the total noise level at frequency j.

Boundary Layer Calculations The boundary layer parameters used in the noise prediction model are computed at each element using the XFOIL viscous-inviscid panel code.

2.3. Geometry Parameterization Model

The blade geometry was parameterized by using Bézier curves to describe the blade chord and twist distributions and airfoil sections. A flexible fitting algorithm was implemented to fit any airfoil shape into two curves for the pressure and suction sides.

3. Implementation

In this section, a description of the developed prediction tool is presented, followed by its validation.

3.1. Aeroacoustic Prediction Tool

The aerodynamic, aeroacoustic and parameterization models described in the previous section were implemented in an prediction tool, using C++ and Python programming languages. The prediction tool is robust and flexible, allowing the configuration of the simulations in detail.

3.2. Optimization Framework

The aeroacoustic code was coupled to the Python-based optimization framework pyOpt [7], being chosen the genetic algorithm NSGA-II [8] as the optimization algorithm. From [9], it was found that population number has to be between n and $2n$, with n as the number of design variables, to attain the balance between a good convergence rate and the time spent in the optimization process.

3.3. Validation

In this section, the implemented turbulent inflow noise numerical model is validated and the experimental results from a known axial fan are used to validate and the overall noise spectrum prediction.

Turbulent Inflow Noise Model Validation The computational results obtained by Carolus and Schneider [4] are compared to the ones obtained by the aeroacoustic tool in order to validate the model implementation.

The geometrical details of the fan studied are present in the work already referenced and the input analysis parameters are shown in table 2.

Number of blades	6
Rotational speed (rpm)	3000
Axial flow velocity (m/s)	10.554
Fan diameter (m)	0.299
Hub radius (m)	0.0675
Speed of sound (m/s)	340.46
Air density (kg/m^3)	1.225
Trailing edge angle (deg)	1.858
TE Thickness (% chord)	0.83

Table 2: Analysis parameters for turbulence inflow noise model validation.

The *exact* turbulence parameters values are not provided, it is only stated that the turbulence conditions were under a Natural Inflow classification. The range of values for these conditions is in table 1.

In order to estimate the correct turbulence parameters that produce the same results as the ones from Carolus, a parametric study was conducted

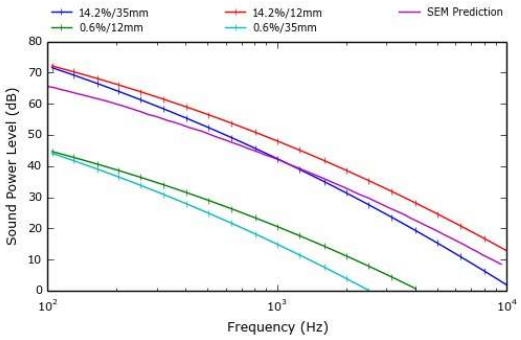

Figure 1: Parametric study to determine the turbulence parameters which have the best fit to the provided data.

for these two variables and the results are presented in figure 1, where the various spectra produced by the tool are compared to the semi-empiric method (SEM) results.

It can be seen that the turbulence intensity influences the overall intensity of the produced noise, while the length scale changes the rate of decay of the spectrum with the frequency. With these conclusions, the best pair of parameters to correlate the two sets of results was found to be 7.5% and 12 mm, for the turbulence intensity and length scale, respectively. In figure 2, the comparison between the two spectra is shown. The correlation is satisfactory and thus the model is validated.

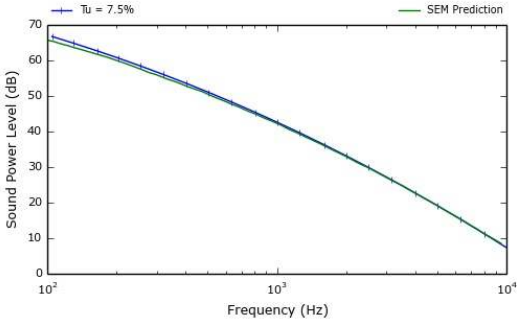

Figure 2: Final validation of turbulent inflow prediction code.

Overall Spectrum Validation The overall spectrum computed by the aeroacoustic tool was compared to experimental results from the same fan used in the turbulent inflow validation. All of the parameters were unchanged, except for the turbulence values, which were changed for TCS+BLR conditions. The observer position was defined as $(x, y, z) = (0, 0, 1)$. The total spectrum with all noise mechanisms is presented in figure 3.

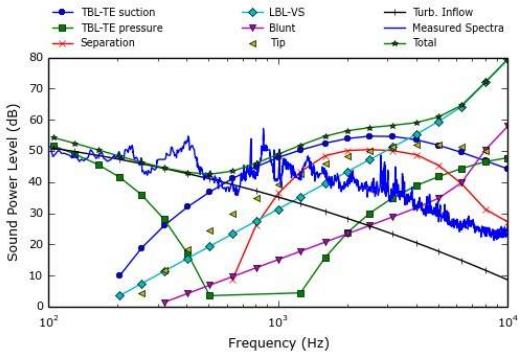

Figure 3: Comparison between experimental and tool computed sound power spectra.

There is a clear overprediction in the high frequency area, which can be explained by the fact that the experimental results are for a ducted fan and the implemented models do not take into account that factor. Since the overprediction is mostly due to the LBL-VS noise mechanism, which can be explained by less vortex shedding in ducted fan than in free space, a new analysis without this mechanism was run and the results are shown in figure 4.

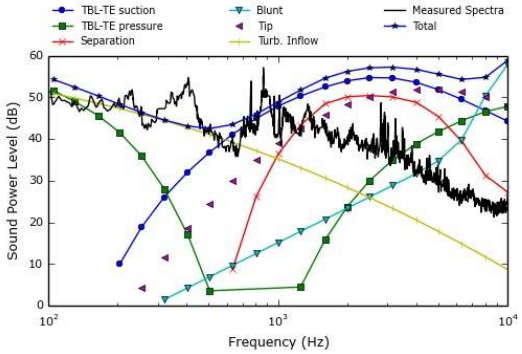

Figure 4: Comparison between experimental and tool computed sound power spectra, without LBL-VS.

The overprediction is still visible, but with lower discrepancy than before. While the overall correlation between the results is sub-optimal, in the area between 100 and 1000 Hz the correlation is satisfactory. Since the zone around 1000 Hz is generally where the produced noise is most intense and the human ear is most sensitive, the model can be considered validated, taking into account the already referred fact that the test fan for comparison is a ducted fan.

4. Results

In this section, the definition of the baseline fan noise levels is described and the results from a geometrical parametric study and several optimization

cases are presented.

The parameters used for the baseline fan characterization were also used in all subsequent analysis.

4.1. Baseline Fan Characterization

In this section, the baseline noise values for the objective fan are determined while establishing the correlation with experimental results.

The geometry of the fan was provided in a 3D CAD format and therefore several airfoil sections had to be extracted from the model in order to input the blade into the aeroacoustic tool. An image of the airfoil sections and their locations is shown in figure 5. The parameters used in the analysis are stated in table 3.

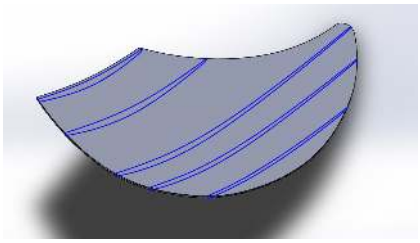

Figure 5: Location of extracted airfoils in the blade model.

Number of blades	3
Rotational speed (rpm)	850
Axial flow velocity (m/s)	10.55
Trailing edge angle (deg)	2
Turbulence intensity (%)	21
Turbulence length scale (m)	0.01

Table 3: Parameters used in baseline fan aeroacoustic analysis.

These parameters were chosen to produce the results with the best correlation with the provided experimental results, with the comparison between both spectra shown in figure 6.

Although there is a slight discrepancy in the mid and high frequency zones, there is a satisfactory overall correlation between the two spectra, which is proven by the baseline noise value of 60.1 dB(A). When compared to the experimental value of 61.4 dB(A), the difference is of 2.1%. Therefore, the baseline fan noise spectrum is characterized, with 60.1 dB(A) as the baseline noise value.

4.2. Geometrical Parametric Study

In this section, the impact of varying the fan diameter and the number of blades in the overall produced noise is analyzed by conducting a parametric study.

When changing these variables, it was assumed that the power consumed by the fan stayed the same. For that to happen, the rotational speed and

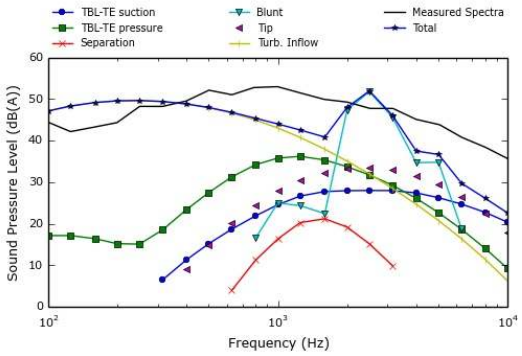

Figure 6: Comparison between computed and experimental spectra of the baseline fan.

the axial flow velocity has to change with the diameter and blade number variation. Therefore, the following relations were used:

$$V = \frac{1.5}{\pi(R_{tip}^2 - R_{hub}^2)} \tag{11}$$

and

$$\Omega_2 = \Omega_1 \left(\frac{N_1}{N_2} \frac{D_1^5}{D_2^5} \right)^{1/3} \quad , \tag{12}$$

where V is the axial velocity, R_{tip} and R_{hub} are the tip and hub radius, respectively , N is the number of blades, D is the diameter and Ω is the rotational speed. The numbers 1 and 2 refer to two different fans.

Also, when changing the blade number, the equivalent area has to stay the same, so that an higher blade number equals to a lower blade chord distribution, such that

$$c_2 = c_1 \frac{N_1}{N_2} \quad . \tag{13}$$

Using these relations, a sequence of simulations were run, where the number of blades was varied between 3 and 6 and the diameter was changed between 400 and 600 mm. The obtained results are shown in table 4, with the noise level of the baseline fan being shown in bold.

It was concluded that by increasing both diameter and blade number can be obtained a reduction in the overall produced noise up to 16.5%.

4.3. Aeroacoustic Fan Optimization

Several single and multi-objective optimizations were performed on the baseline fan and on one of the fans resultant from the parametric study that produce less noise, more specifically, the fan with 500 mm diameter and 6 blades. The objective functions were the OASPL and the fan efficiency. The geometrical design variables were the chord, twist and curvature.

Diameter (mm) \ Blade number	3	4	5	6
400	65.0	64.0	62.1	60.0
450	**60.1**	60.1	58.9	58.4
470	58.5	57.1	59.1	58.6
500	56.9	58.1	57.6	57.2
550	55.3	54.8	53.8	52.3
600	54.2	52.5	51.1	50.2

Table 4: Noise predictions (dB(A)) for different number of blades and diameters.

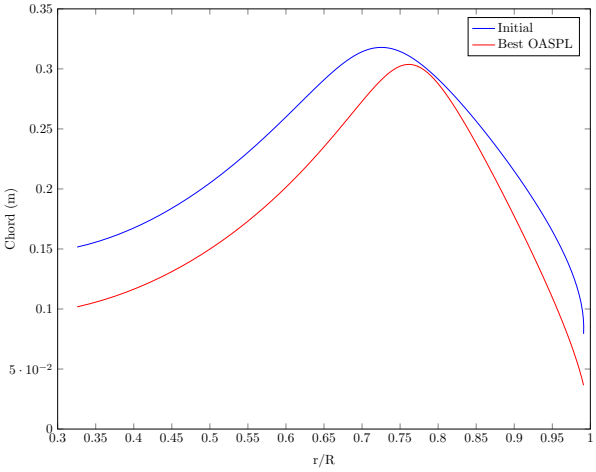

Figure 7: Comparison between the initial and the best OASPL chord distribution.

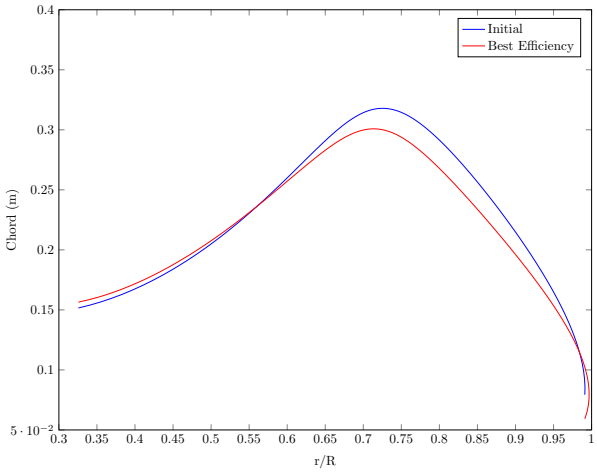

Figure 8: Comparison between the initial and the best efficiency chord distribution.

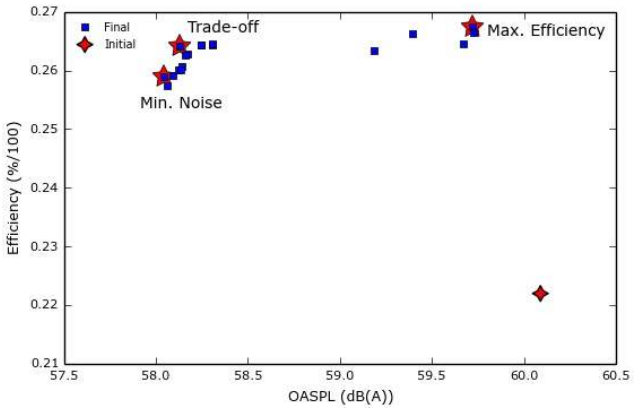

Figure 9: Pareto front in chord multi-objective optimization case.

4.3.1 Baseline Fan

Chord The first optimization to be considered is the optimization of the blade chord. The chord distribution is defined by a 6^{th} order Bézier curve and since the locations of the curve control points are the design variables, except for the radial coordinates of endpoints, the total number of design variables for the chord optimization is 10. In all analyses, the chord values and radial positions were constrained between 90% and 110% of their initial values:

$$\begin{aligned} 0.9\ c_i^{initial} < y_i^{cp} < 1.1\ c_i^{initial} \\ 0.9\ \frac{r_i}{R_{max}} < x_i^{cp} < 1.1\ \frac{r_i}{R_{max}} \end{aligned} \tag{14}$$

The first objective was the OASPL and the optimization resulted in a decrease of the noise down to 58.42 dB(A), using the optimized chord distribution shown in figure 7.

A second optimization was conducted, with the efficiency as the objective function, which resulted in an increase up to 26.1%. The optimized chord distribution is presented in figure 8.

The final chord optimization had both the OASPL and efficiency as objective functions. The optimizer provided a set of solutions from a dispersed set and the resulting Pareto front is presented in figure 9. The trade-off solution results in an OASPL of 58.25 dB(A) and an efficiency of 26.4% and the respective chord distribution is shown in figure 10.

Twist The second main design variable is the blade twist. The twist distribution is defined by a 5^{th} order Bézier curve and the design variable procedure is the same as the one in the chord optimization, which results in a total number of 8 design variables.

In all twist optimizations, the twist values were constrained between 85% and 115% of their initial

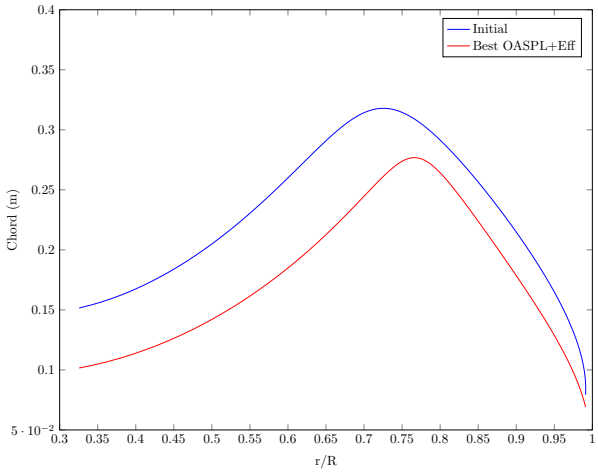

Figure 10: Comparison between the initial and the trade-off solution chord distribution.

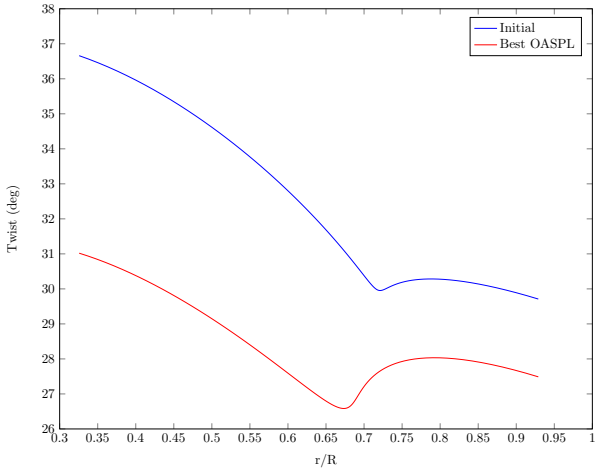

Figure 11: Comparison between the initial and the best OASPL twist distribution.

values, being the radial positions constraints the same as the ones in the chord optimization:

$$\begin{aligned} 0.85\ \theta_i^{initial} < y_i^{cp} < 1.15\ \theta_i^{initial} \quad , \\ 0.9\ \frac{r_i}{R_{max}} < x_i^{cp} < 1.1\ \frac{r_i}{R_{max}} \quad . \end{aligned} \tag{15}$$

In the OASPL optimization, the optimal solution resulted in a noise reduction down to 59.25 dB(A) and the respective twist distribution is shown in figure 11.

In the optimization for the efficiency objective function, the obtained results showed an increase of 2.3% to 24.5%, with the optimized twist distribution shown in figure 12.

In the twist optimization of both objective functions, OASPL and Efficiency, the optimizer produced the Pareto front shown in figure 13. The twist distribution for the trade-off solution is presented in figure 14.

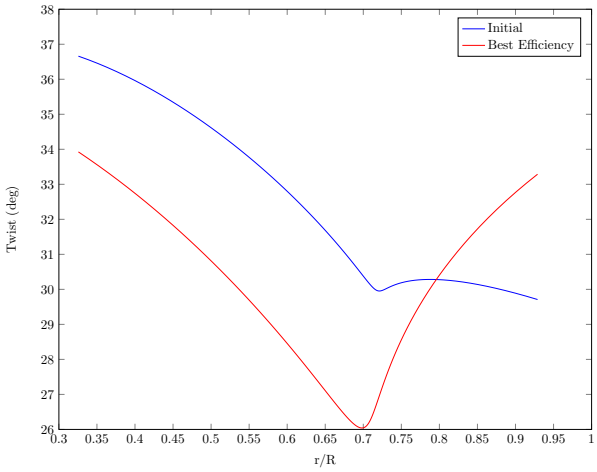

Figure 12: Comparison between the initial and the best efficiency twist distribution.

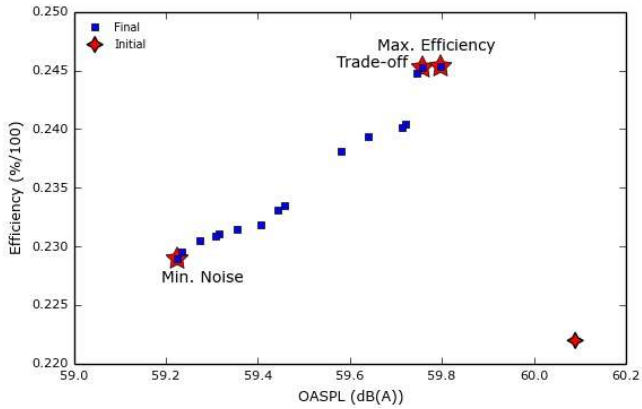

Figure 13: Pareto front in twist multi-objective optimization case.

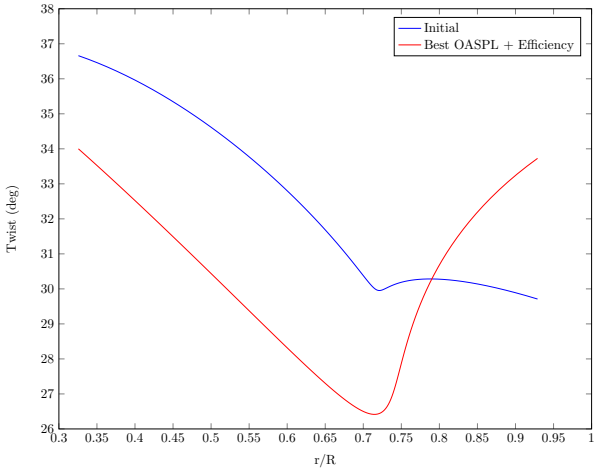

Figure 14: Comparison between the initial and the trade-off twist distribution.

# of Airfoil	Baseline chord %	Optimized chord %
1	71.5	79.54
2	64.5	72.3
3	42.8	43.06
4	43.33	37
5	40.39	34

Table 5: Curvature optimization results.

Curvature Curvature is the third and last design variable to use in the optimization process. In this case, only the impact in the noise was addressed, since one of the disadvantages of the BEM theory is that the blade elements are considered independent among themselves, with the fan efficiency unaffected by the change in the blade curvature.

The curvature is defined by the locations of the control airfoil sections in relation to an axis that goes through the blade along the radial direction. These locations are constrained between -10% and +10% of their initial positions expressed in percentage of chord. The obtained results by the optimizer showed a minimal decrease to 60.03 dB(A) and the respective control sections locations are presented in table 5.

Chord and Twist With the chord and twist being considered simultaneously as design variables, the solutions obtained by the optimizer for each objective function, separately, resulted in a decrease in OASPL of 4.1% to 57.61 dB(A) and in an increase in efficiency of 5.3% to 27.5%. The respective chord and twist distributions for each case are presented in figures 15 and 16.

Chord, Twist and Curvature In the optimization with the combination of all design variables, it was expected that the combined effect would produce the best results. However, it was observed that by coupling the curvature with the twist and chord, the noise improvement brought by the latter combination was diminished, being the final result a reduction to 57.85 dB(A). The resulting chord and twist distribution will not be presented, due to fact that it is similar to the one shown in figure 15, proving the negative impact the curvature has when combined with chord and twist changes.

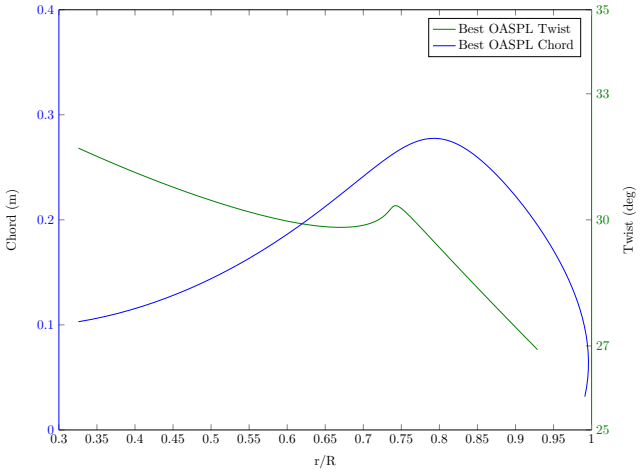

Figure 15: Chord and twist distribution for best OASPL.

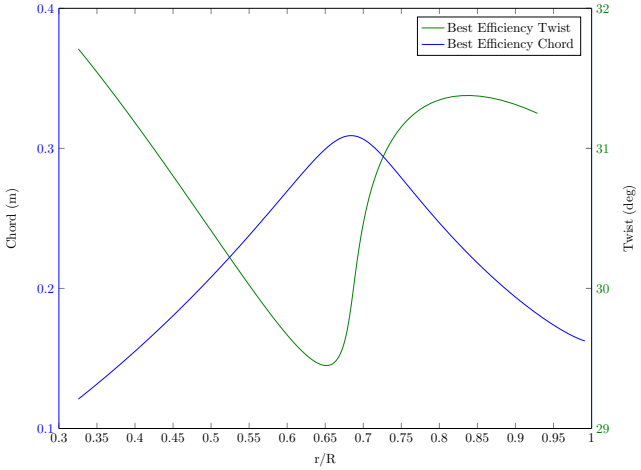

Figure 16: Chord and twist distribution for best efficiency.

Summary of the Results A summary of all the presented optimization results is shown in table 6, where it can be seen that the solution involving the change of the chord and twist simultaneously produces the best overall results. It presents the minimum noise, with 57.61 dB(A), which equals a 4.1% reduction, the maximum efficiency, for an increase of 5.3% to 27.5% and the best trade-off, if the criteria is the minimum ratio between the noise and efficiency. The terms C, T and Curv, refer to chord, twist and curvature, respectively,

4.4. Improved Fan

The optimization process for the 500 mm and 6 blade fan was followed exactly like in the baseline fan optimization. Therefore, only a summary of the results obtained is presented in table 7. For reference, the noise and efficiency baseline values for this fan are 52.3 dB(A) and 1.7%, respectively. Similarly to the baseline fan optimization, the com-

Design Variable	OASPL (dB(A))	Efficiency (%)	OASPL + Eff
C	58.42	26.1	58.25/26.4
T	59.25	24.5	59.79/24.5
C+T	57.61	27.5	59.33/27.9
Curv	60.03	-	-
C+T+Curv	57.85	-	-

Table 6: Summary of the optimization results for the baseline fan.

Design Variable	OASPL (dB(A))	Efficiency (%)	OASPL + Eff
C	50.08	2.2	50.56/1.7
T	51.78	1.9	51.75/1.7
C+T	49.64	4.1	51.15/2.6
Curv	52.19	-	-
C+T+Curv	49.60	-	-

Table 7: Summary of the optimization results for the 500 mm diameter/6 blades fan.

bination of design variables, chord and twist, produced the best overall results, with a decrease of 5.2% in the noise for the minimum OASPL case, an increase of 2.4% in efficiency in the maximum efficiency case and with the best trade-off solution.

In figure 17, the radial distribution of noise for the baseline fan and the two optimized fans is presented. In each image, the frontal view of the fan is shown, being the hub depicted by the white circle in the center. The azimuthal angles are shown outside the outer circle, with the fan radius scale being set up along the circle radius. The noise reduction towards the optimized improved fan can be seen by the difference in scales in each figure.

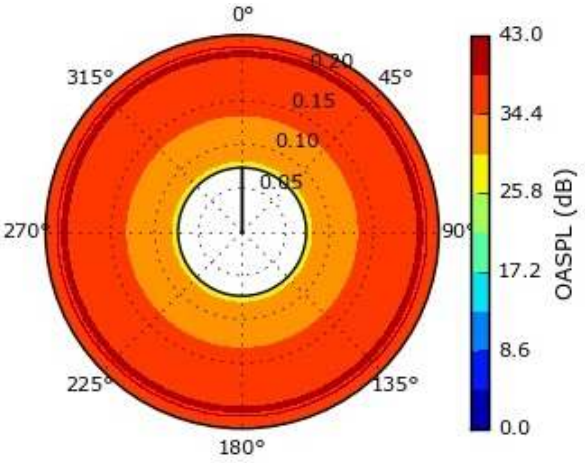

(a) Baseline Fan

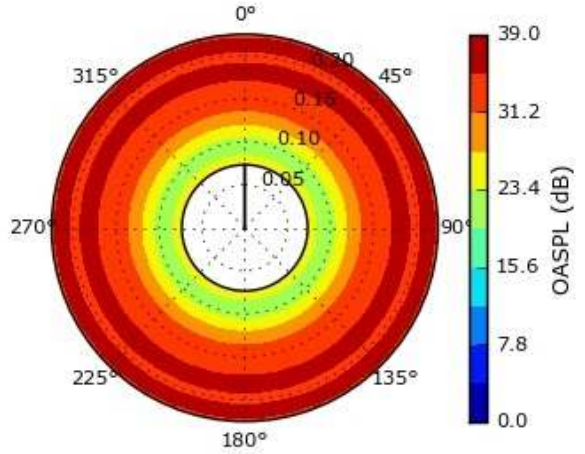

(b) Optimized Baseline Fan

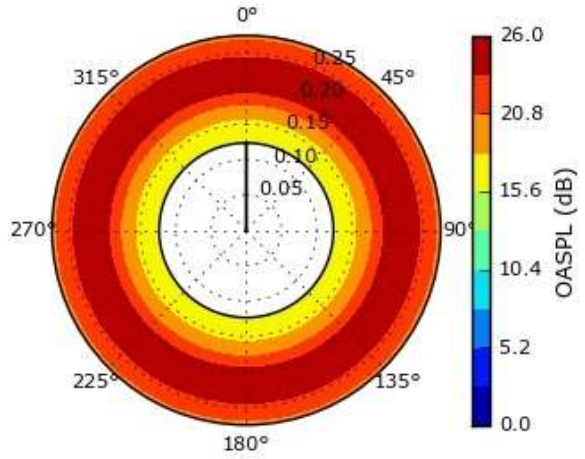

(c) Optimized Improved Fan

Figure 17: Noise radial distribution of the rotor for different optimization cases.

5. Conclusions

In the developed work, a custom wind turbine aerodynamic and aeroacoustic prediction code was successfully adapted for axial flow fans. These adaptations were also validated against experimental data of a known axial fan.

An existing fan geometrical model was parameterized and introduced into the aeroacoustic tool, using Bézier curves to describe the chord and twist distributions and the cross sectional airfoil shapes.

Using the capabilities of the developed aeroacoustic framework, the baseline noise values of the fan were defined. A parametric study was conducted,

where the impact of the fan diameter and blade number on the produced noise was assessed. From this study, it was concluded that an increase in both diameter and blade number results in a noise reduction up to 16.5%. Regarding the efficiency, the diameter increase improves it, while the increase in blade number has a severe negative impact in the aerodynamic performance, reaching values as low as 1.7%.

The aeroacoustic code was successfully integrated into an optimization framework, which allows for optimal solutions to be found for various optimization problems.The blade chord, twist and curvature were optimized in single and multi-objective optimization problems in order to find the minimum noise, maximum efficiency and trade-off solutions. The optimization algorithm was applied to two fans: the baseline fan and the fan which produced less noise from the parametric study. In the baseline fan, a maximum reduction of 4.1% in OASPL and a maximum increase of 5.3% in efficiency was achieved, while in the second fan, the OASPL was reduced by 5.2% and the efficiency increased 2.4%. In both cases, the combination of design variables which produce these results is the blade chord and twist.

When comparing the new fan with the baseline fan, a total reduction of 17.5% in the OASPL is obtained, but at a cost of decreasing the efficiency by 18.1%. Given the conclusions obtained in this work, the most realistic approach in obtaining the best trade-off solution would be to increase the diameter to 550 mm, maintain the number of blades and change the chord and twist to reach an optimal solution.

Acknowledgements

The author would like to thank Prof. André Calado Marta for his teachings, patience, availability and for being an overall excellent supervisor throughout the development of this thesis. Also, the author would like to express a special appreciation to Prof. Luís Braga Campos for his valuable input and scientific review during various stages of this work.

References

[1] B. Berglund and P. Hassmn. Sources and effects of low-frequency noise. *Acoustical Society of America*, 99(5):2985–3002, May 1996.

[2] L. Bommes, J. Fricke, and R. Grundmann. *Ventilatoren*, pages 352–377. Vulkan Verlag, 2. auflage edition, 2003.

[3] T. F. Brooks, D. S. Pope, and M. A. Marcolini. Airfoil self-noise and prediction. Technical report, National Aeronautics and Space Administration, 1989.

[4] T. Carolus, M. Schneider, and H. Reese. Axial flow fan broad-band noise and prediction. *Journal of Sound and Vibration*, 300:50–70, July 2007.

[5] Z. Du and M. Selig. A 3-D stall-delay model for horizontal axis wind turbine performance prediction. In *Proceedings of the 1998 ASME Wind Energy Symposium, Reno, NV*, pages 9–19, 1998.

[6] H. Glauert. Airplane propellers. In *Aerodynamic Theory*, pages 169–360. Springer Berlin Heidelberg, 1935.

[7] R. E. Perez, P. W. Jansen, and J. R. R. A. Martins. pyOpt: A python-based object-oriented framework for nonlinear constrained optimization. *Structures and Multidisciplinary Optimization*, 45(1):101–118, 2012.

[8] K. D. A. Pratap, S. Agarwal, and T. Meyarivan. A fast and elitist multiobjective genetic algorithm: Nsga-ii. *IEEE Transactions on Evolutionary Computation*, 6(2):182–197, 2002.

[9] S. S. Rodrigues. Aeroacoustic optimization of wind turbine blades. Master's thesis, Instituto Superior Técnico, Nov. 2012.

[10] I. J. Sharland. Sources of noise in axial flow fans. *Journal of Sound and Vibration*, 1(3):302–322, 1964.

[11] L. Viterna and D. Janetzke. Theoretical and experimental power from large horizontal-axis wind turbines. Technical report, U.S. Department of Energy, Conservation and Renewable Energy, Wind Energy Technology Division, 1982.